Solution Structure of Oxidized Rat Microsomal Cytochrome b_5 in the Presence of 2 M Guanidinium Chloride: Monitoring the Early Steps in Protein Unfolding[†,‡]

Fabio Arnesano, Lucia Banci, Ivano Bertini,* and Dionysios Koulougliotis

Department of Chemistry, University of Florence, Florence, Italy

Received June 30, 1998; Revised Manuscript Received September 1, 1998

ABSTRACT: One- and two-dimensional proton NMR spectroscopy has been employed in order to study the denaturation effect of guanidinium chloride (GdmCl) on the oxidized state of the A-form of rat microsomal cytochrome b_5 (cyt b_5). The protein rapidly starts losing the heme at denaturant concentrations larger than ∼2.0 M and a largely unfolded protein is eventually obtained. An estimate of the unfolding kinetics is obtained and, by use of a two-state model (folded ↔ unfolded), a value for $\Delta G°$. Below this concentration, small (≤0.15 ppm) but systematic chemical shift variations take place for the diamagnetic as well as the hyperfine-shifted signals, indicating that some structural changes occur. However, the protein core maintains its overall structure. The analysis of the two-dimensional nuclear Overhauser effect spectroscopy (2D NOESY) maps has allowed the determination of the solution structure of the protein in the presence of 2 M GdmCl. By use of 1199 meaningful NOESY constraints (obtained from the assignment of 75% of the total protons) and 166 pseudocontact shifts, a family of 40 structures has been obtained through the program PSEUDYANA. The family was further refined through restrained energy minimization and the final root mean square deviation (RMSD) values with respect to the average structure are 0.67 ± 0.10 Å and 1.14 ± 0.11 Å for the backbone and heavy atoms, respectively. The quality of the present structure is equivalent to that of the one obtained recently for the native form [Arnesano et al. (1998) *Biochemistry 37*, 173−184], thus allowing a meaningful comparison between the two structures. Upon addition of 2 M GdmCl, significant local structural differences are induced to the protein backbone segments comprising residues 33−38 (helix α2) and 62−64 (end of helix α4−beginning of helix α5) while the overall folding scheme of the protein is still maintained. These protein regions form part of the "pocket" supporting the heme, whose plane is also rotated by approximately 10° around an axis connecting the C_2 and C_8 carbon atoms. The initial steps of the unfolding process involve breaking of a few hydrogen bonds that stabilize local structural conformations. The hydrogen bond between Ser 64 and propionate 7, which stabilizes the heme binding to the protein frame, is broken in the presence of 2 M GdmCl. The same occurs for two hydrogen bonds between two β-strands (β2 and β3), thus inducing the disruption of one of the antiparallel β-sheets forming one side of the heme cavity. Our results are critically discussed in connection with the native-state protein local backbone mobility characteristics and point to the backbone carbons of Glu 37 and Ser 64 being the first "breaking points" of the protein frame once the global unfolding reaction is initiated at a somewhat higher concentration of denaturant.

The study of the structural characteristics of proteins under nonnative conditions is increasingly attracting interest since it can provide valuable insights into several significant issues of modern biophysics: the relationship between the primary sequence and tertiary structure, protein stability and turnover, transmembrane protein transport, and protein recognition (*1*−*3*). Recent technological advances in NMR spectroscopy have made it one of the most useful techniques applied for the structural characterization of denatured or partially unfolded states (*4*−*14*)**.** In this work, we have been interested in studying the effect of the denaturant guanidinium chloride (GdmCl) on the structural properties of the oxidized form of rat microsomal cytochrome b_5 (cyt b_5).

Cyt b_5 is an amphipathic protein consisting of a hydrophilic (heme-containing) and a hydrophobic (membrane-bound) segment, located in the endoplasmic reticulum of hepatic cells (*15*). It is an ubiquitous protein in many living organisms and its heme-containing component is involved in a wide variety of biological processes (*16*−*21*). In addition, this hydrosoluble part is efficiently expressed in *Escherichia coli* (*15*), retaining fully its activity (*22*) and consequently it provides an excellent model system for a variety of biophysical studies. The protein is present in solution in two forms known as A and B, the main difference between the two being a 180° rotation of the heme plane

[†] This work was supported by the European Community (TMR-LSF Contract ERBFMGECT950033, Program BIOMED, CT BMH4-CT96-1492), by Italian CNR (Biotecnologie e biologia molecolare, CTB CNR 95.02860.CT14) and by MURST-ex 40%. D.K. thanks the TMR Program of the European Union for a postdoctoral fellowship (Contract ERBFMBICT960994).

[‡] The structure coordinates described in this paper have been deposited in the Brookhaven Protein Data Bank (ID code 1blv).

* Corresponding author: Department of Chemistry, University of Florence, Via Gino Capponi 7, 50121, Florence, Italy. Fax +39-55-2757555; tel +39-55-2757549; e-mail bertini@lrm.fi.cnr.it.

10.1021/bi981546p CCC: $15.00
Published on Web 11/10/1998

around the α,γ-*meso*-carbon atoms. The ratio between these two forms varies depending on the organism producing the protein. In the case of the expressed rat microsomal isoenzyme, this ratio is approximately 60:40 (A:B). For the latter isoenzyme, the solution NMR structures of the A form have been determined for both the reduced (*23*) and oxidized (*24*) states, as well as that of the B form for the oxidized state (*25*). The NMR structure has also been determined for the A and B forms for the reduced state of the bovine isoenzyme (*26*). The A-form, being more abundant (≥60%), is more easily amenable to biophysical characterization. It is also on this form that our attention is focused in the present study.

In the past two decades, the denaturation of cyt b_5 has mainly been studied in terms of its thermal unfolding characteristics via the use of differential scanning calorimetry, circular dichroism (CD), and resonance Raman and absorption spectroscopies (*27*−*30*). One of the earliest studies that stimulated those that followed involved the denaturation characteristics of cyt b_5 upon addition of GdmCl (*31*). In that study, CD and optical absorption as well as gel chromatography were employed in order to follow the denaturation process of the detergent-solubilized (d-b_5) and the tryptic fragment (t-b_5) cyt b_5 purified from rabbit liver microsomes. It should be noted that d-b_5 corresponds to cyt b_5 containing both the hydrophilic (heme-containing) and the hydrophobic components, while t-b_5 contains only the heme-containing component and is thus analogous to the soluble cyt b_5, whose NMR solution structure is available and is the subject of the present investigation. In the study of Tajima et al. (*31*), the denaturation of d-b_5 proceeded as a two-stage process, the first transition occurring at about 2.6 M and the second at 5.0−5.5 M GdmCl concentrations. On the contrary, the denaturation of t-b_5 proceeded as a one-stage process at a GdmCl concentration of about 2.9 M. This one-stage GdmCl-induced denaturation of t-b_5 seemed to be correlated with the detachment of the heme, which was followed independently and found to occur at a GdmCl concentration of 2.6−2.9 M. In the present study, we have been interested in characterizing, via NMR spectroscopy, the structural changes occurring in the protein frame of the hydrophilic (water-soluble) component of the A form of rat microsomal cyt b_5 before the global unfolding reaction is initiated (i.e., in almost subdenaturing concentrations of denaturant). Since we provide a structural characterization of the system in equilibrium with its native state, we should note that the structural changes observed are not necessarily related to a kinetically competent intermediate in the early stages of unfolding. The presence of such kinetic unfolding intermediates, accumulated in the millisecond (or faster) time scale, has been evidenced during the unfolding of horse cytochrome *c* in the oxidized state via stopped-flow far-UV circular dichroism as well as fluorescence quenching (*32*). On the other hand, no accumulation of such intermediates was evidenced in a recent study of the unfolding process of the small (85-residue) globular protein HPr (histidine-containing phosphocarrier protein) (*33*). In the latter case, both kinetic and equilibrium experiments could be adequately described as a two-state process. In the present study, our aim has been that of identifying the protein regions that are more sensitive to the attack of GdmCl and, as a result, to gain some insight on the mode of action of denaturants causing protein unfolding.

MATERIALS AND METHODS

Sample Preparation. Rat microsomal cyt b_5 was isolated, using the previously described procedure (*15*), from cultures of *E. coli* strain NM-522 harboring the recombinant pUC13 plasmid containing the gene encoding the 98 amino acid polypeptide corresponding to the soluble part of the microsomal cyt b_5 (kindly provided by Dr. S. G. Sligar). About 20 mg of protein, as obtained from the last purification step, were exchanged through ultrafiltration with 100 mM aqueous phosphate buffer, and the pH was gradually adjusted to 7.0. The final concentration was approximately 3 mM with a sample volume of approximately 500 μL. Under these conditions the majority of the protein (>95%) is in the oxidized form. A 7 M solution of GdmCl was prepared in 100 mM phosphate buffer and its pH was adjusted to 7.0 by the addition of small quantities of NaOH. Aliquots of this GdmCl solution were added to the NMR sample in successive steps in which the following concentrations of denaturant were achieved: 0.5, 1, 1.5, 1.6, 1.7, 1.8, 1.9, 2.0, 2.1, 2.2, 2.3, 2.4, 2.6, and 2.8 M. The protein was exchanged with D_2O via successful washes with a 100 mM phosphate buffer in D_2O (pD 7.0) containing 2 M GdmCl.

NMR Spectroscopy. ^{1}H NMR experiments were performed on a Bruker DRX 500 NMR spectrometer operating at a proton nominal frequency of 500.13 MHz. One-dimensional (1D) NMR experiments using a spectral width of 60 ppm and a short recycle time (520 ms) in order to optimize detection of the hyperfine shifted signals were performed after each addition of GdmCl. Two-dimensional (2D) NOESY spectra were acquired for GdmCl concentrations equal to 1.0, 1.5, 2.0, and 2.4 M. Two types of NOESY spectra were obtained for each of the four GdmCl concentrations: a "diamagnetic" spectrum with 15 ppm spectral width and 100 ms mixing time, in order to optimize signal detection in the diamagnetic region and a "paramagnetic" spectrum with 60 ppm spectral width, 25 ms mixing time and relatively short recycle time (390 ms) in order to optimize detection of fast relaxing signals. In the "diamagnetic" spectra, the WATERGATE sequence (*34*) or presaturation was used to suppress the strong H_2O resonance. Only presaturation for H_2O suppression was used during the acquisition of the "paramagnetic" spectra. Quadrature detection was achieved by using the time-proportional phase incrementation (TPPI) method (*35*). The diamagnetic data consisted of 4K data points in the acquisition dimension and of 730 experiments in the indirect dimension. The corresponding numbers were 2K and 600 for the paramagnetic data. The raw data were weighted with a squared cosine function, zero-filled, and Fourier-transformed to obtain a final matrix of 4K × 1K and 2K × 1K data points for the diamagnetic and paramagnetic spectra, respectively. A polynomial baseline correction was applied in both dimensions. All spectra were collected at 298 K. Data processing was done by using the standard Bruker software and analyzed on IBM RISC 6000 computers with the program XEASY (*36*).

Proton−*Proton Distance and Pseudocontact Shift Constraints.* The solution structure was determined for the A-form of oxidized cyt b_5 in the presence of 2 M GdmCl.

The majority of the peaks used for the structure calculations (≈80%, see later) were integrated in the NOESY map acquired over the diamagnetic window at 298 K in H_2O by using the WATERGATE sequence for solvent suppression, while approximately 12% of the dipolar connectivities were integrated in the diamagnetic NOESY map collected with water presaturation. In this map, the strong resonance of GdmCl (6.86 ppm) is also saturated as its protons exchange fast with those of the bulk water, thus allowing the resolution of all NOESY connectivities in the range between 6.1 and 7.2 ppm. Dipolar connectivities involving hyperfine-shifted protons were integrated in the NOESY spectrum acquired over the 60 ppm spectral window. Intensities of dipolar connectivities were converted into upper distance limits, to be used as input for structure calculations, by using the approach provided by the program CALIBA (*37*). Connectivities measured in NOESY maps acquired with different mixing times were calibrated independently. The calibration curves were adjusted iteratively as the structure calculations proceeded. Stereospecific assignments of diastereotopic protons were obtained from the program GLOMSA (*37*).

Pseudocontact shifts (δ_{pc}) were employed as additional constraints for the structure calculations. The pseudocontact contribution to the chemical shift arises from the magnetic susceptibility anisotropy of the metal ion and depends on the position of a given nucleus with respect to the principal axes of the magnetic susceptibility tensor and on the inverse third power of its distance from the metal ion. Therefore, pseudocontact shifts can be used as long-range structural constraints (*38*−*41*). Pseudocontact shifts were obtained by subtracting from the chemical shifts of the oxidized form of cyt b_5 in the presence of 2 M GdmCl those of the native reduced form available at 313 K (*23*). A tolerance of 10% was used in the PSEUDYANA calculations (see later) with a minimum value of 0.3 ppm for the nonexchangeable protons and 0.5 for the NHs. The hyperfine shifts of the heme and of the axial to the heme ligands (His 39 and His 63) were not included in the calculations since they would experience a nonnegligible contact shift.

Structure Calculations. The structure calculations were performed with PSEUDYANA (*42*), which is the modified version of the program DYANA (*43*) made suitable to include pseudocontact shifts as additional restraints. A preliminary family of 20 structures obtained from only the NOE constraints was used as an input model to the program FANTASIAN (*44*, *45*) to provide the initial values of $\Delta\chi_{ax}$ and $\Delta\chi_{rh}$. These calculations were performed for each of the 20 preliminary structures, and the average values of $\Delta\chi_{ax}$ and $\Delta\chi_{rh}$ were used as starting values in the PSEUDYANA structure calculations. It should be noted that the PSEUDYANA protocol needs only the initial values of the magnetic susceptibility tensor anisotropies and not its direction cosines; i.e., no specific initial orientation is provided for the tensor. A special residue, called LTNS, formed by dummy atoms is used to define the position of the metal center and the directions of the magnetic susceptibility tensor in the dihedral angle coordinate space. The dummy atoms of this residue have their van der Waals radii set to zero so that it can freely penetrate into the protein. An upper distance limit of 0.2 Å was set between the pseudoatom defining the metal ion and the iron atom. The location of this residue and the tensor orientation were optimized during the structure calculations.

The heme group was included in the calculations by defining a new residue in the amino acid library that was bound to the protein frame through special linkers, using the same previously described procedure (*24*). The two binding histidines (His 39 and His 63) are coordinated to the iron atom through upper distance limits of 2.1 Å between the iron and the Nϵ2 of the two His residues. After each cycle the magnetic anisotropies were evaluated and used as input for the following calculation until the final values did not deviate more than 5% from the initial ones. The relative weight of the two types of constraints was kept equal. Three hundred random structures were annealed in 12 000 steps using the above constraints. The 40 structures with the lowest target function constitute the family of structures.

Restrained energy minimization (PSEUDOREM) was then applied to each member of the family using the AMBER package (*46*). The distance constraints were applied within the molecular mechanics and dynamics module of Sander and the pseudocontact shifts were included as constraints by means of the module PCSHIFTS (*45*). The force field parameters for the heme and its ligands, as well as the overall calculation procedure, were set up as previously reported for similar systems (*24*, *47*). The initial values of the magnetic susceptibility anisotropy used as input in PSEUDOREM were the output of the PSEUDYANA runs. After the end of the PSEUDOREM runs (2 cycles) they were subjected to a less than 3% change from their initial values.

The quality of the structure was evaluated in terms of deviations from ideal bond lengths and bond angles and through Ramachandran plots obtained with the programs PROCHECK (*48*) and PROCHECK-NMR (*49*).

Structure calculations and analyses were performed on IBM RISC 6000 computers.

Computer-Aided Assignment. Once a quite well-defined family of structures was available from the DYANA calculations, the program CORMA (*50*) was employed in order to assist in the assignment of the NOESY cross-peaks. They were, however, all individually checked. The new NOESY cross-peaks found through CORMA analysis amounted to 13% of the total number of peaks used as input in CALIBA.

RESULTS AND DISCUSSION

NMR Titration with GdmCl. The changes in chemical shift value and intensity of the paramagnetic resonances were followed by titrating the native oxidized cyt b_5 protein with increasing amounts of GdmCl. This was done via 1D ^{1}H NMR experiments after each addition of an aliquot of GdmCl solution into the NMR protein sample. In the range of GdmCl concentrations used (0−2.8 M), the chemical shift values of the paramagnetic resonances displayed small but reproducible systematic changes of about 0.10−0.12 ppm. The majority of these peaks showed downfield shifts with the exception of two methyl peaks (3-CH_3 and 5-CH_3) that displayed upfield shifts. Concomitant with these shift changes, a decrease in intensity of the paramagnetically shifted signals is observed. At 2.8 M GdmCl concentration the paramagnetically shifted signals have less than 10% of their original intensity. An examination of the diamagnetic part of the 1D NMR spectrum showed significant loss of the spectral resolution and remarkable coalescence of the resonances toward the "center" (0−8 ppm) of the spectrum.

The small but systematic chemical shift changes indicate the presence of an exchange equilibrium between two species, which is fast with respect to the chemical shift separation of the individual resonances in the two interconverting forms. In addition to this fast exchange, a certain percentage of the protein is also found in its largely unfolded state during the titration. Indeed, the decrease in signal intensity suggests that at high GdmCl concentrations, the b-type heme of cyt b_5 is getting detached from the protein frame. This is also consistent with the results of Tajima et al. (*31*), where it was shown that protein denaturation and heme detachment are characterized by the same transition midpoint (equal to 2.9 M GdmCl), suggesting that the two processes occur simultaneously. The formation of a largely unfolded state is evidenced by a ^{1}H−^{15}N heteronuclear single quantum coherence (HSQC) spectrum obtained after addition of 2.0 M GdmCl, where a set of new cross-peaks is present, which are characteristic of an unfolded state since the majority of them are located in the "central" region of the spectrum (7.9−8.3 ppm for the ^{1}H chemical shifts). One of such new cross-peaks is, however, resolved outside the huge envelope at 10.17 and 136.6 ppm for the ^{1}H and ^{15}N chemical shifts, respectively. Careful analysis of the ^{1}H 1D NMR spectra showed the gradual appearance of this signal in the course of the titration with GdmCl. In 2D homonuclear NOESY spectra obtained at 2.4 M GdmCl and 100 ms mixing time, a relatively strong exchange (EXSY) cross-peak was obtained between this proton resonance and the NH resonance of Lys 72. By measuring the cross-peak and the diagonal-peak intensities and assuming a symmetrical two-site exchange, an exchange rate on the order of 0.5−0.7 s^{-1} is estimated between the unfolded and the native-like state. In the ^{1}H 2D NOESY spectrum at 2 M GdmCl, this exchange cross-peak was of very small intensity and practically very difficult to differentiate from the noise level. This is partly due to the lower absolute intensity of the signal in the unfolded state and partly to the fact that at lower GdmCl concentration the interconversion rate between the native and unfolded protein is even slower than 0.5 s^{-1}.

In addition to the changes in chemical shift, the intensity changes resulting from the addition of GdmCl were also followed for the paramagnetically shifted resonances. All resonances showed the same dependence, and the average signal intensity as a function of GdmCl concentration is shown in Figure 1. We can notice that the slope of the curve remains relatively constant (equal to ∼−0.2 M^{-1}) up to ∼2 M concentration of GdmCl and then increases drastically. This type of behavior has been observed before via NMR for a different protein (*33*) and has been fitted to a two-state N ↔ U model (N, native; U, unfolded), according to (*32*, *51*, *52*)

$$y_{obs} = \{y_N + \alpha_N[\text{GdmCl}] + y_U + \alpha_U[\text{GdmCl}]\exp\{(-\Delta G^\circ + m[\text{GdmCl}])/RT\}\}/\{1 + \exp\{(-\Delta G^\circ + m[\text{GdmCl}])/RT\}\} \quad (1)$$

where the symbols have the following meanings: y_{obs} is the normalized signal intensity so that it is equal to 1 at 0 M GdmCl concentration. [GdmCl] is the GdmCl concentration, $R = 8.3143$ J K^{-1} mol^{-1}, and y_N, y_U, α_N, and α_U represent intercepts and slopes of the native (N) and unfolded (U) baselines, respectively. ΔG° represents the free energy of unfolding in the absence of denaturant, while m is a parameter reflecting the steepness of the unfolding transition. If this type of analysis is performed for the present system, we obtain from the least-squares fit $\Delta G^\circ = 29 \pm 3$ kJ mol^{-1} and $m = 11 \pm 1$ kJ mol^{-1} M^{-1}. In addition, the transition midpoint, c_M, which is the GdmCl concentration at which 50% of the protein is unfolded, is estimated to be equal to 2.6 ± 0.3 M. The value obtained for ΔG° is very similar, within experimental error, to the one obtained before (25 ± 2 kJ mol^{-1} at the same temperature) in a study of the thermal unfolding of the tryptic fragment of cyt b_5 purified from rabbit liver microsomes via scanning calorimetry (*27*). The same holds for the transition midpoint, which for the tryptic fragment of rabbit liver cyt b_5 was found to be 2.9 M at pH 7.5 (*31*) via circular dichroism spectroscopy.

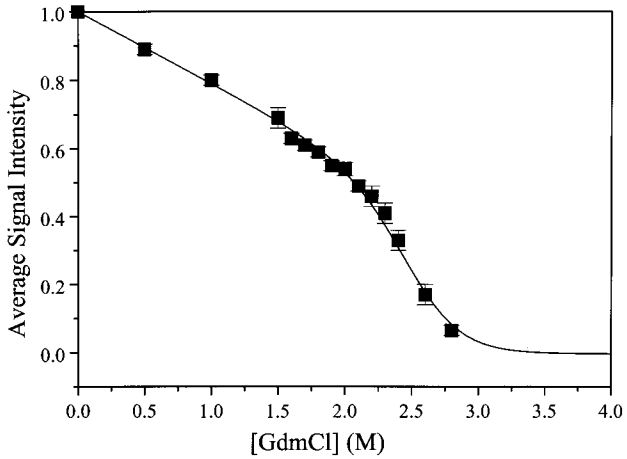

FIGURE 1: Change in average signal intensity of the paramagnetically shifted resonances of the A form of oxidized rat microsomal cytochrome b_5 as a function of GdmCl concentration. The solid curve represents a fit of the normalized experimental intensities to eq 1.

Even though the experimental data on signal intensity can be fitted to a two-state model, the actual mechanism of the unfolding transition is more complicated, as described above (see also Discussion for reference to other systems). Our NMR titration data provide evidence for at least two exchange processes occurring simultaneously: a fast one with respect to the chemical shift separation, as indicated by the chemical shift changes, between the native protein and a native-like "intermediate" produced by the addition of denaturant; and a slow one (with respect to the chemical shift separation), at relatively low denaturant concentrations, between the native-like system and the unfolded state. This second process corresponds to the global unfolding reaction and is expected to become much faster at higher (>2.4 M) GdmCl concentrations.

In our experiments, after addition of 2.8 M GdmCl, the concentration of denaturant was decreased 10-fold by adding to the sample a specific quantity of its "native-state" buffer (100 mM phosphate, pH 7.0). The sample solution was then left overnight at 4 °C and subsequently its volume was decreased 10-fold via centrifugation with Centricon tubes (3000 MW cutoff). The 1D NMR spectrum obtained after this process was identical, within experimental error, to the one taken in the beginning of the NMR titration before addition of GdmCl, thus showing the reversibility of its effect on the structure of oxidized rat microsomal cyt b_5. The

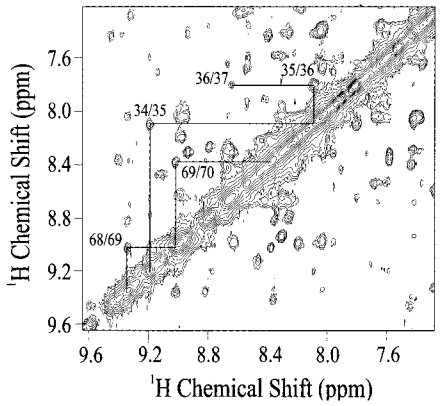

FIGURE 2: NH−NH region of the WATERGATE NOESY spectrum of oxidized rat microsomal cytochrome b_5 in the presence of 2.0 M GdmCl acquired at 500 MHz, 298 K, and pH 7.0. The sequential NH−NH connectivities involving residues 68−70 and 34−37 are depicted as a representative example.

above-described NMR titration and protein refolding experiments were performed twice and the data were completely reproducible.

In this study, we are interested in characterizing the local structural changes occurring in the protein frame as it is "prepared" for the global unfolding reaction with the increasing concentration of added denaturant. Thus, on the basis of the titration behavior, we chose to characterize the oxidized A-form of cytochrome b_5 in the presence of 2 M GdmCl.

Sequence-Specific Assignment. The sequence-specific assignment of the ^{1}H NMR spectrum of cyt b_5 in the presence of 2 M GdmCl was done by taking into account the extensive assignment already available for the native oxidized form (*24*). The systematic change in the chemical shift values of the protein spin systems was followed by analyzing the 2D NOESY maps obtained at 1.0, 1.5, and 2.0 M concentrations of GdmCl. A sample of the NH−NH region in the WATERGATE NOESY map with 100 ms mixing time in the presence of 2.0 M GdmCl is shown in Figure 2. The majority of the proton resonances experienced a downfield shift on the order of 0.1−0.2 ppm. The resonances with downfield shifts larger than 0.3 ppm were Hδ of Tyr 7 (−0.35 ppm), Hδ1 of His 39 (−0.53 ppm), NH of His 63 (−0.46 ppm), and 1-CH_3 (−0.90 ppm) and Hα-*meso* (−0.51 ppm) of the heme. The resonances with the larger upfield shifts were NH of Leu 9 (0.13 ppm) and 3-CH_3 (0.20 ppm) and Hγ-*meso* (0.26 ppm) of the heme. The total number of the assigned residues is 88, which resulted in 75% of the total protons. In the native form, the total number of assigned residues was 89, corresponding to 78% of total protons (*24*). The complete ^{1}H assignment is available as Supporting Information.

Secondary Structure. The elements of secondary structure can be identified by analyzing the pattern of the assigned NOESY cross-peaks (*53*). Helical structures are characterized by a high number of sequential and medium-range connectivities such as $d_{NN}(i, i+1)$, $d_{NN}(i, i+2)$, $d_{\alpha N}(i, i+3)$, $d_{\alpha N}(i, i+4)$, and $d_{\alpha\beta}(i, i+3)$. Six elements of helical structure are predicted from this analysis and they involve the following residues: 9−13, 32−39, 43−50, 55−63, 65−75, and 81−87. β-Strands are expected to give strong $d_{\alpha N}$ sequential and intraresidue connectivities and weak d_{NN} connectivities. In our case, this applies for the following residue segments: 2−8, 21−25, and 28−30. These results are quite similar to those found for the native form of the same protein, indicating that even in the presence of 2 M GdmCl the secondary structural elements are retained.

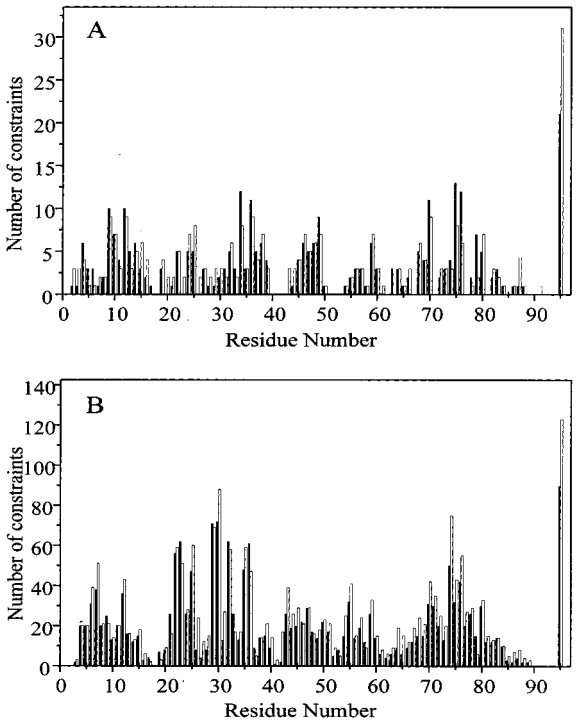

FIGURE 3: Number of intraresidue (A) and interresidue (B) meaningful NOE-derived constraints used in the structural calculations of the A-form of oxidized rat microsomal cyt b_5 in the presence of 2 M GdmCl (solid bars). The numbers of constraints used for the structural calculations of the native form [taken from Arnesano et al. (*24*)] are also displayed (open bars) for comparison. Residue 95 represents the connectivities involving the heme.

Hydrogen/Deuterium Exchange Behavior. The H/D exchange behavior of the amide protons was checked 5 days after the sample was exchanged with D_2O. Nonexchanging amide protons were found for 21 residues in the following stretches: 4−5, 12−14, 21, 33, 36−38, 48, 50−51, 55−56, 59−60, 62, 66, and 69−70.

Solution Structure Calculations. From the 2D NOESY maps, 1538 experimental constraints were assigned and integrated. Of these, 1237 were found in the NOESY map acquired with 100 ms mixing time and using the WATERGATE pulse sequence in order to suppress the water resonance, 193 were in the map collected with the same mixing time but using presaturation to achieve solvent suppression, and 108 were from the NOESY map in which a 25 ms mixing time was employed. Of the total 1538 experimental distance constraints, 1199 were found to be meaningful (an average of 13.6 per assigned residue) and were used in the structure calculations together with the 166 pseudocontact shifts. Residues 1−3 and 88−94 belong to unstructured domains of the protein. The average meaningful NOE constraints were 14.2 per residue in the segment 4−87. The meaningful NOE constraints per residue are shown in Figure 3 (filled bars), together with those of the native form of the same cytochrome (open bars, taken from ref *24*) for comparison. As seen in Figure 3, the number of NOE constraints is comparable, even though for the majority of

residues (70% of the total) it is lower in the protein sample where the denaturant was present. This explains the lower number of NOEs per assigned residue in the present case (13.6 relative to 15.5 for the native form). At the same time, the number of interresidue NOEs is observed to be higher for 14 residues (16% of the total) in the presence of 2 M GdmCl relative to the native form. These residues are the following: 9, 17, 19, 21, 23, 29, 32−33, 36, 46, 48, 53, 58, and 79. A total of 17 stereospecific assignments were obtained through the program GLOMSA (*37*) during the course of the calculations, and six iterations of PSEUDYANA were performed before the magnetic anisotropy tensor reached convergence. The resulting family of 40 structures has RMSD values to the mean structure (RMSD values will hereafter always refer to the mean structure, unless specified otherwise) of 0.69 ± 0.10 Å and 1.14 ± 0.11 Å for backbone and heavy atoms, respectively (calculated for residues 4−84). The target function lies in the range of 0.32−0.90 Å^2 (average target function of 0.73 ± 0.14 Å^2). In the end of the calculations there are no consistent violations of either the NOE or the pseudocontact shift constraints. The contribution of the pseudocontact shift constraints with respect to that of the NOEs to the target function is approximately 5%.

Restrained energy minimization (PSEUDOREM) yields a family with an average penalty function of 50 ± 8 kJ mol^{-1} (28.79−68.48 kJ mol^{-1}), corresponding to a target function of 0.37 ± 0.06 Å^2 (0.22−0.51 Å^2), the contribution of pseudocontact shifts being lower than 12% compared to that of the NOE constraints. The average RMSD decreases slightly (0.67 ± 0.10 Å) for the backbone atoms while it remains the same for the heavy atoms. Analysis of the quality of the 40-structure family was done by using the program PROCHECK-NMR (*49*). The results of this analysis together with several other standard parameters used to assess the structure quality are reported in detail in Table 1. The good quality of the structure can be concluded by inspection of this table.

Table 1: Restraints Violations and Structural and Energetics Statistics for the Solution Structure of Oxidized Rat Microsomal Cytochrome b_5 in the Presence of 2 M GdmCl[a]

	PSEUDOREM (40 structures)	⟨PSEUDOREM⟩
RMS Violations per Experimental Distance Constraint[b] (Å)		
intraresidue (301)	0.023 ± 0.004	0.023
sequential (226)	0.012 ± 0.003	0.010
interresidue short range ($1 < \|i - j\| \leq 5$) (254)	0.011 ± 0.003	0.005
interresidue long range ($\|i - j\| > 5$) (418)	0.014 ± 0.003	0.019
total (1199)	0.016 ± 0.002	0.017
Average Number of Violations per Structure		
intraresidue	12 ± 2	12
sequential	4 ± 2	3
interresidue short range ($1 < \|i - j\| \leq 5$)	5 ± 2	2
interresidue long range ($\|i - j\| > 5$)	8 ± 2	9
total	29 ± 4	26
violations larger than 0.3 Å	0.25	0
violations between 0.1 and 0.3 Å	10 ± 3	10
largest violation (Å)	0.36	0.24
Energy of Nonbonded Interactions (kJ mol^{-1})		
	−5700 ± 400	−5823
Structural Analysis[c]		
residues in disallowed regions (%)	3 ± 1	1.4
residues in generously allowed regions (%)	5 ± 2	4.3
residues in additionally allowed regions (%)	24 ± 3	24.3
residues in most favored regions (%)	68 ± 3	70
no. of bad contacts/100 residues	0.02	0
H-bond energy (kJ mol^{-1})	3.5 ± 0.2	3.47
overall *G*-factor	−0.36 ± 0.05	−0.38

[a] PSEUDOREM indicates the energy-minimized family of 40 structures; ⟨PSEUDOREM⟩ is the energy-minimized average structure obtained from the coordinates of the individual PSEUDOREM structures. [b] The number of experimental constraints for each class is reported in parentheses. [c] The program PROCHECK−NMR (*49*) was used to assess the overall quality of the structure. For the PROCHECK statistics, less than 10 bad contacts per 100 residues, an average hydrogen-bond energy in the range of 2.5−4.0 kJ mol^{-1}, and an overall *G*-factor larger than −0.5 are expected for a good quality structure.

The solution structure of the A-form of oxidized cyt b_5 in the presence of 2 M GdmCl is characterized by high resolution, comparable to that of the native form, even in regions close to the paramagnetic center (Figure 4). The RMSD values per residue for the backbone and heavy atoms are reported in Figure 5A. The resonances of Ser 18 were not assigned [as also in the native form (*24*)], and as a result, this residue is not well-defined. The N (1−3) and C-terminal (85−94) ends are also characterized by poor resolution due to the lack of a sufficient number of interresidue NOE connectivities. The program PROCHECK, which relies on the Kabsch and Sander algorithm (*54*) has been used to assign the secondary structure elements of the protein. Six helices have been found comprising the following residues: 8−13, 34−38 (3_{10} type), 43−50, 55−62, 64−72, and 81−86, which correspond to helices α1−α6 found also in the native form (*24*). The corresponding helical segments found in the latter form were 8−14, 33−39, 42−50, 54−62, 64−74, and 81−87, which are practically equivalent to the ones in the present structure. The β-strand elements identified with PROCHECK in the present structure comprised residues between 21 and 25 and between 28 and 32, which are equivalent to strands β3 and β4 of the native structure forming an antiparallel β-sheet, "supporting" the four helices (α2−α5) that constitute the heme binding pocket. The strands β1 and β2, identified in the native structure in the segments 5−7 and 75−78, are not readily assigned by PROCHECK in the present structure. In our case, residues 2−7 belong to the core β region of the Ramachandran plot; however, no specific secondary structural element is being assigned by the program. As far as the 75−78 segment is concerned, only 75 is assigned as making part of a β-sheet, while the remaining three residues are set to make part of an S-bend.

Comparison with the Structure of the Native Form. The solution structure of the A-form of oxidized rat microsomal cyt b_5 has recently been solved by NMR (*24*) and this allows a detailed comparison with its structure after the addition of 2 M GdmCl, determined in this work. This can be done by superimposing the average energy-minimized structures of the two proteins and thus calculating the RMSD values between the two. Subsequently, these values have to be compared with the RMSD values that define the two families. The global RMSD values between the two averaged minimized structures are 1.49 and 2.01 Å for backbone and heavy atoms, respectively. The RMSD per residue is reported in

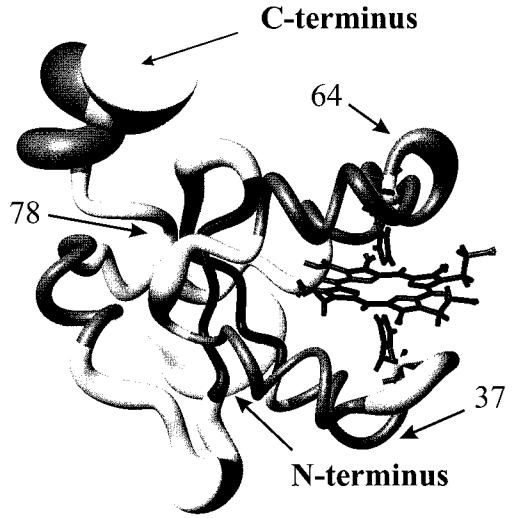

FIGURE 4: PSEUDOREM family of 40 structures of the A-form of oxidized rat microsomal cyt b_5 in the presence of 2 M GdmCl. The figure was generated with the program MOLMOL (*68*), and the radius of the tube is proportional to the RMSD. The positions of Glu 37, Ser 64, Gly 77, and the N- and C-termini are shown with arrows.

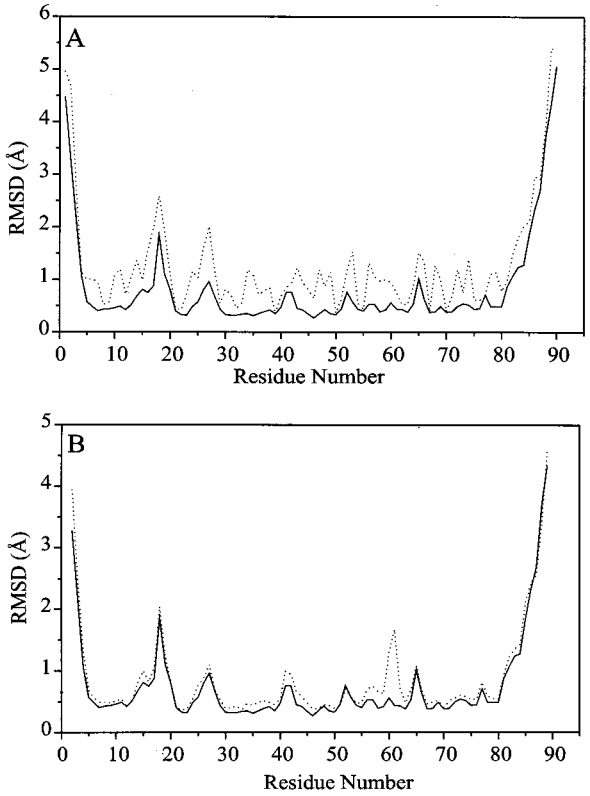

FIGURE 5: (A) RMSD values per residue to the mean structure, for the PSEUDOREM family of structures for backbone (solid line) and for all heavy atoms (dotted line). (B) Backbone RMSD values per residue to the mean structure, for the PSEUDOREM (solid line) and the REM (dotted line) 40-structure families.

Figure 6 (thick solid line) and it is compared to the RMSD per residue for each family [native (thin dotted−dashed line) and in the presence of 2 M GdmCl (thin dotted line)] and the sum of the RMSD values of the two families (thick dotted−dashed line), either superimposing the whole structures (A) or only three residues at a time (B). As can be seen in Figure 6, the structure definition within each family of structures is overall very good and is comparable between

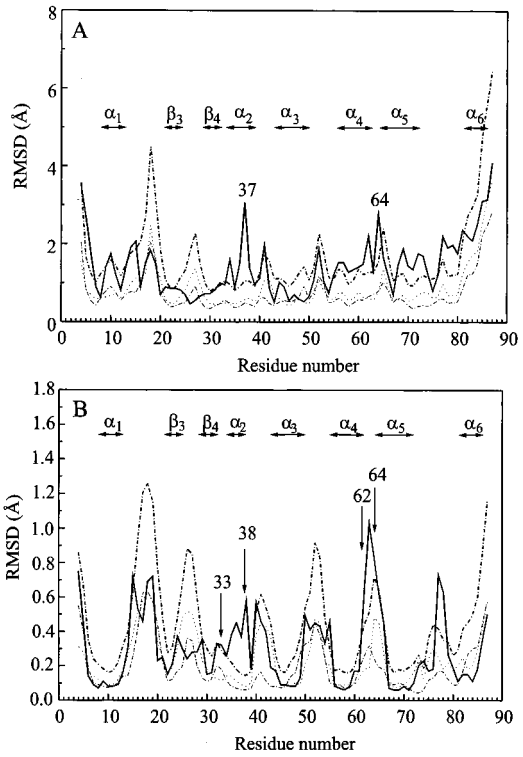

FIGURE 6: RMSD per residue for backbone atoms within the 40-structure families of the native oxidized cyt b_5 [taken from Arnesano et al. (*24*), thin dotted−dashed line], oxidized cyt b_5 in the presence of 2 M GdmCl (thin dotted line), and between the average energy-minimized structures of the two families (thick solid line) superimposing either the whole structures (A) or only three residues at a time (B). The sum of the RMSD values per residue for the two families of structures is also shown (thick dotted−dashed line). The positions of the α-helices and β-strands are also shown.

the two families. Consequently, a meaningful comparison can be undertaken.

The first observation that can be made is that there are three regions in the protein sequence where the RMSD between the two average minimized structures is significantly larger than the RMSD of each family, irrespective of the way that the superimposition has been done (i.e., the whole structures or three residues at a time). This applies also if one compares the sum of the RMSD values of the two families (thick dotted−dashed line) with the RMSD between the two average minimized structures (thick solid line). These regions include residues 33−38, 62−64, and 77−78. The first two segments belong to the helices that form the heme binding pocket (α2, α4, and α5). The third segment is located between helices α5 and α6, which in the native form is part of a β-sheet (β2), while in the presence of 2 M GdmCl this secondary structure element is not readily formed. On the other hand, the residue segments between 9−11 and 13−15 display a large RMSD between the two average minimized structures only when these two are superimposed globally (Figure 6A). This means that, upon addition of 2 M GdmCl, these residues are undergoing a global small translational displacement while their local conformations are well maintained. The conformational changes that are induced to the protein segments comprising residues 33−38, 62−64, and 77−78 can be described as follows. The first segment (33−38) constitutes helix α2 and shows a displacement away from its neighboring helix α3 (which remains structurally intact). The maximum deviation from

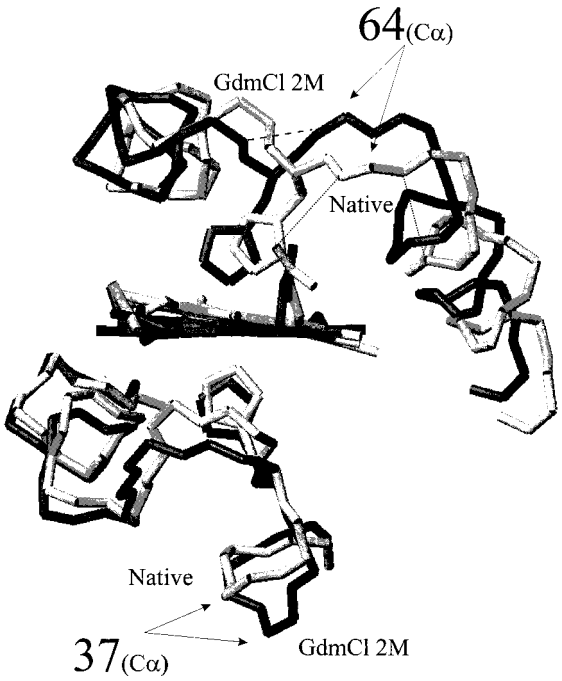

FIGURE 7: Backbone drawing of the A-form of oxidized rat microsomal cyt b_5 in its native form (gray) and in the presence of 2 M GdmCl (black). The protein segments comprising residues 35−50 and 55−74, as well as the heme, are denoted. The positions of the Cα carbon atoms of Ser 64 and Glu 37 are shown with arrows. Three relevant hydrogen bonds are indicated between the following atom pairs: NH of Ser 64−carboxylate oxygen of propionate 7 (dotted line, left), CO of Ser 64−NH of Ala 67 (dotted line, right), and NH of Ser 64−CO of Gly 62 (dashed line). The hydrogen bonds denoted with dotted lines are present only in the native form of the protein (gray backbone), while the third one (dashed line) is absent in the native form and is formed upon addition of 2 M GdmCl (black backbone).

the initial position is observed, among the backbone atoms, for the backbone Cα atom of Glu 37 (3.15 Å) located at the end of the helix. In the second segment (62−64) the backbone atom with the largest deviation from the initial position is the Cα of Ser 64 (3.52 Å), corresponding to a bending movement of the backbone bringing closer the atoms of residues 62 and 64. The helices to which Gly 62 and Ser 64 belong (α4 and α5, respectively) remain otherwise intact. Together with the movement of these two segments, a significant rotation of the heme plane is taking place. The ring rotates by approximately 10° around an axis connecting the C_2 (pyrrole A) and C_8 (pyrrole Δ) carbon atoms. The heme atom showing the largest movement from its initial position is the carbon of methyl 5-CH_3 (1.53 Å). This movement is followed also by the axial ligands, which also in the present case remain essentially perpendicular to the heme plane. The concerted movement involving the segments 33−38 and 62−64 and the heme plane described above, constitutes the major structural difference induced to the A-form of rat microsomal cyt b_5 upon addition of 2 M GdmCl. It is displayed in detail in Figure 7. The above presented structural differences are supported by differences in the experimental NOE constraints available for the two forms of the protein. An extensive comparison of the two sets of experimental constraints showed differences either in their identity (dissappearance or appearance of new NOESY cross-peaks upon addition of denaturant) or their intensity. For example, in the protein region 33−38, a new NOESY cross-peak was identified between the Hβ proton of Glu 37 and the Hα proton of Thr 33. The Hβ and HN protons of Thr 33 displayed in their turn two new NOESY cross-peaks with the Hε proton of His 15 and the Hβ proton of Leu 46, respectively. In the protein region comprising residues 62−64, Ser 64 lost its interresidue connectivities with Thr 65 and Asp 66. However, three new NOESY cross-peaks are present between the HN proton of Ser 64 with the Hβ and Hγ protons of Arg 68 and the Hγ proton of Glu 59. The proton−proton distances corresponding to the NOESY cross-peaks present only in one form were checked in both average minimized structures. These distances were in all cases larger than 7 Å for those cross-peaks that are missing in one of the two forms. In addition, significant changes in NOE intensities, therefore translating into different interproton distances, were observed for certain residues. One of the most dramatic cases is the increase of the NOESY cross-peak intensity between the Hα proton of Glu 59 and the HN proton of His 63 upon addition of 2 M GdmCl. The upper distance limits produced by CALIBA are 5.5 and 3.5 Å in the native and the present structures, respectively, and the corresponding interproton distances in the two average minimized structures are 5.0 and 2.5 Å.

The structural changes induced by addition of 2 M GdmCl likely result from the breaking of some hydrogen bonds that connect different residues in the protein frame and determine the conformation of some parts of the protein. Particularly relevant is the hydrogen bond between the carboxylate of propionate 7 and the backbone NH of Ser 64. This hydrogen bond has been proposed to be relevant for the stabilization of the heme binding to the protein frame (*55*, *56*). In the X-ray crystal structure of the A-form of the oxidized bovine isoenzyme (*57*), the distance between the backbone nitrogen atom of Ser 64 and the closest carboxylate oxygen atom of propionate 7 is 2.9 Å. In our solution structure of the A-form of the oxidized rat microsomal isoenzyme (*24*), the corresponding distance in the average structure is larger (5.7 Å); it shows, however, relatively significant scattering within the 40-conformer family (2.6−8.1 Å), thus indicating that several conformers of the family experience this hydrogen bond. Most importantly, the presence of experimental NOEs between the β-protons of propionate 7 and the NH of Ser 64 also supports the partial time-averaged existence of this hydrogen bond. Addition of 2 M GdmCl produces an increase of about 3 Å between the carboxylate oxygen (Oδ1) of propionate 7 and the peptidic NH of Ser 64, resulting thus in the definite breaking of this stabilizing interaction. Consequently, the protein backbone moves away from the heme and changes its conformation. As shown in Figure 7, the structural change induced to the protein backbone segment comprising residues 62−64 results in a rearrangement of the local hydrogen-bonding network. In addition to the hydrogen bond with propionate 7, also the hydrogen bond between the CO atom of Ser 64 and the NH of Ala 67 is broken, while a new hydrogen bond between the NH of Ser 64 and the CO atom of Gly 62 is created upon addition of denaturant. The pattern of the local rearrangement of the hydrogen-bonding network described above is shown in Figure 7. In the protein segment made up by residues 33−38, no key hydrogen bond for determining the tertiary structure is present. However, an extensive network of hydrogen bonds connects the residues belonging to helix α2

(residues 32−38) and several of these are broken in the presence of 2 M GdmCl. Consequently, small local rearrangements occur along the backbone that propagate in order to create the final effect.

The significant conformational change induced to the backbone carbons of Glu 37 and Ser 64 indicates that these residues are the first to "feel" the stress resulting from the addition of denaturant. As a result, they adapt their local position in a way such that the helices supporting the heme maintain their conformations and probably constitute the first structural breaks induced in the protein frame once the global unfolding reaction (at a somewhat higher GdmCl concentration) is initiated.

Finally, the structural change observed for the segment 77−78 is a bending movement of the backbone by approximately 30−40° and is located in a protein region close to the C-terminus where the structure is getting progressively less defined. This change is most likely a consequence of the breaking of two strong hydrogen bonds between two β-strands (β2 and β3) that form an antiparallel β-sheet in the native structure. More specifically, the hydrogen bonds between the NH of Val 29 and the CO of Gly 77 and between the CO of Val 29 and the NH of Gly 77 are not present upon addition of 2 M GdmCl. This produces a displacement of the 77−78 protein segment away from the sheet denoted as β3 (residues 28−32).

Comment on the Pseudocontact Shift Constraints. Extensive structure calculations were also performed by using only the NOE distance constraints in order to estimate the extent to which the addition of the nonstandard pseudocontact shift constraints increase the structure definition and in general the effect they have in the calculation. The average RMSD values of the family of 40 structures obtained after the restrained energy minimization without the inclusion of pseudocontact shifts (REM) are 0.81± 0.10 and 1.29 ± 0.12 Å for the backbone and heavy atoms, respectively. Figure 5B reports the average backbone RMSD values for the two 40-structure families [REM (dotted line) and PSEUDOREM (solid line)] and it shows that the inclusion of the pseudocontact shifts in the structural calculations increases the resolution mainly close to the paramagnetic center and especially in the regions 41−42, 56−57, and 60−62. The RMSD values between the average structures of the two families are 0.43 and 0.82 Å fot backbones and heavy atoms, respectively, and therefore lie within the precision achieved for each family. These data indicate that the inclusion of the pseudocontact shifts has the positive effect of increasing the resolution of the solution structure and at the same time does not introduce any changes in the overall and local folding of the protein in comparison with that obtained by taking into account only the NOE constraints in the calculations. The use of pseudocontact shifts is particularly significant in systems such as the present one, where the number of NOEs is smaller than in the native protein, and could therefore be determinant for obtaining well-resolved solution structures in cases where the experimental conditions are such that a low number of standard constraints is produced.

The $\Delta\chi_{ax}$ and $\Delta\chi_{rh}$ values calculated over the final 40-structure family are $(3.00 \pm 0.10) \times 10^{32}$ and $(-1.09 \pm 0.07) \times 10^{32}$ m^3, respectively. The *z* axis of the magnetic susceptibility tensor makes an angle of 11° ± 6° with the perpendicular to the heme plane, while the *x* axis makes an angle of 22° ± 15° with the α−γ-*meso* direction. The values reported as errors correspond to three standard deviations. The corresponding angles found in the minimized average structure were 11.4° and 25.6°, respectively, and they are identical within the error to those found for the family of 40 structures. The values of $\Delta\chi_{ax}$ and $\Delta\chi_{rh}$ in the present system are very close to the ones found for the native form of the enzyme (*24*) [$(2.83 \pm 0.02) \times 10^{32}$ and $(-1.06 \pm 0.01) \times 10^{32}$ m^3, respectively]. In the native form of the protein, the angles that the *z*- and *x*-axis make with the perpendicular to mean heme plane and the α−γ-*meso* direction are 2.5° and 12.7°, respectively (*24*). The directions of the magnetic axes with respect to the heme frame are slightly different upon addition of 2 M GdmCl. However, the uncertainty in the pseudocontact shifts (due to the lack of the chemical shifts of the reduced form in the presence of GdmCl) creates a relatively large uncertainty also on the values of the angles describing the directions of the magnetic axes and thus prevents us from a meaningful comparison.

Denaturant-Induced Differential Hydrogen Exchange Behavior. Upon addition of GdmCl at a 2 M concentration, there is a change in the protein stretches that are protected against D_2O exchange (in the days time scale) relative to those already observed for the native form (*24*). More specifically, the amide protons belonging to the stretches constituting the β3 (*28*−*32*) and β4 (*21*−*25*) sheets become more readily exchangeable. This is in contrast with what was observed in both the reduced and the oxidized forms of the native protein (*24*). In the latter two cases, the increased protection of these β-sheets was justified in terms of a fairly rigid structural unit responsible for providing a solid scaffold for the four helices forming the heme crevice. Even though the average structural characteristics of these two β-sheets remain unchanged upon addition of 2 M GdmCl, their differential H/D exchange behavior is indicative of an increase in local mobility.

On the other hand, the α2 (33−39) and α4 (54−62) helices display in the present system an increased protection against D_2O exchange relative to the native form in the same oxidation state. Four and five protons of the helices α2 and α4, respectively, display slow exchange behavior, while the corresponding numbers were zero and one in the native oxidized form. These experimental observations would indicate a decrease in the local mobility of these two α-helical elements.

Denaturant-Induced Structural Changes and Cyt b_5 Mobility in the Micro- to Millisecond Time Scale. The local backbone mobility of the reduced and oxidized native forms of rat microsomal cyt b_5 in the micro- to millisecond time range has recently been studied via ^{15}N rotating-frame relaxation measurements ($R_{1\rho}$) (*58*). The majority of the backbone nitrogens of helix α3 (44−49) and several belonging to helices α4 (54, 58−60) and α5 (67, 69, 72, 74) were shown to have high mobility in the oxidized form of the protein. Among the four helices forming the heme pocket, α2 was the least mobile. It is interesting to note that the protein segments which experience the largest structural changes upon addition of 2 M GdmCl (33−38, 62−64, and 77−78) belong to protein regions that do not display significant mobility (in the micro- to millisecond time range) in the native oxidized form. This would indicate that the

most rigid parts of cyt b_5 are the ones that more likely "feel" first the effect of the denaturant and thus constitute the initial targets of its action. In consequence, it may be inferred that at low denaturant concentrations (i.e., before the global unfolding reaction has started) the most mobile parts of the protein skeleton can relatively easily rearrange in order to accommodate the structural changes induced by the presence of the denaturant molecules, while this is not the case for the less mobile regions. These results corroborate the "native-state hydrogen exchange" theory presented recently (*59*), where it was shown that the amide hydrogens that are more readily involved in local "opening" reactions (i.e., the "fast" hydrogens) are less susceptible to GdmCl attack at low concentrations. On the other hand, the effect of denaturant at low concentrations is readily observed for the "slowest hydrogens".

Comparison with the Unfolding Events in Other Cytochromes. Among the cytochromes whose folding/unfolding process has been followed either with kinetic and/or with equilibrium experiments, the most studied is horse cytochrome *c* (refs *32* and *60* and references therein). Studies have also been done on yeast cytochrome *c* (*61*, *62*) as well as cytochrome c_2 from photosynthetic bacteria (*63*). The kinetic studies have provided evidence for the accumulation of multiple kinetic intermediates during unfolding, even if the data obtained in experiments done at equilibrium could be fitted by assuming a two-state model. Concentrating on horse cytochrome *c*, the studies done so far are consistent with the disruption of the bond between one of the axial heme ligands (Met 80) and the iron ion and its substitution with another ligand as being the first step in the unfolding process (*63*−*66*). In the present case, we deal with cytochrome b_5, whose heme moiety is not covalently attached in the protein frame as in *c*-type cytochromes and could thus be expected to present a different unfolding behavior. The experimental data are obtained at equilibrium and at relatively low denaturant concentration. Consequently, the structural changes observed might not necessarily correlate with kinetic changes occurring in denaturing concentrations of denaturant. Even though they point against a bond disruption between the axial ligands and the iron ion taking place in the early steps of protein unfolding, this suggestion has to be tested by further studies. It is interesting to notice, on the other hand, that the recent native-state hydrogen exchange studies on oxidized horse cytochrome *c* (*59*) showed that the indole NH of Trp 59, which in the native state is hydrogen-bonded to one of the carboxylate oxygens of the heme propionate 7 (*67*), is involved in a quite large unfolding reaction upon addition of GdmCl. This effect is analogous to what was found in the present study, i.e., the complete disruption of the Ser 64−propionate 7 hydrogen bond, which in the native form is, on time average, partially present. From the above considerations, a possible central role of propionate 7 in cytochrome unfolding is inferred. The generality of this statement has to await further experimental testing.

Concluding Remarks. In the present work, specific backbone structural changes taking place upon addition of denaturant to oxidized cyt b_5 at a "critical" concentration preceding the global unfolding reaction have been identified. These changes are localized on the protein backbone regions comprising residues 33−38, 62−64, and 77−78, which are consequently proposed to be the initial targets of the denaturant action. Guanidinium chloride is breaking important structural hydrogen bonds, thus producing structural changes in these regions. The breaking of two hydrogen bonds between two β-strands in the 77−78 residue fragment induces the disruption of the β-sheet that constitutes one side of the heme pocket. In the neighborhood of the heme, the complete disruption of the structurally relevant hydrogen bond between Ser 64 and the carboxylate of propionate 7 produces a dramatic movement of the protein backbone in the 62−64 residue fragment. The loss of this stabilizing interaction involving propionate 7 (whose conformation remains unchanged) could possibly be the reason also for the subsequent rotation of the heme plane. In addition to the structural changes, indirect experimental evidence indicates that GdmCl at 2 M concentration induces changes to the local protein backbone mobility as well as evidenced by the increased number of exchanging NHs. In either case (structural or mobility change) the protein regions that "feel" the action of the denaturant are rigid in the micro- to millisecond time scale in the native form (*58*). The global unfolding action of GdmCl at concentrations larger than 2.0 M is also explored and some kinetic and thermodynamic data have been obtained.

ACKNOWLEDGMENT

We thank Dr. Isabella C. Felli for valuable help and discussions at the initial stages of this work.

SUPPORTING INFORMATION AVAILABLE

Four tables, listing the ^{1}H chemical shifts, experimental NOE intensities, stereospecific assignments, and pseudocontact shifts used for the structure calculations (45 pages). Ordering information is given on any current masthead page.

REFERENCES

1. Dill, K. A., & Shortle, D. (1991) *Annu. Rev. Biochem. 60*, 795−825.
2. Shortle, D. R. (1996) *Curr. Opin. Struct. Biol. 6*, 24−30.
3. Smith, L. J., Bolin, K. A., Schwalbe, H., MacArthur, M. W., Thornton, J. M., & Dobson, C. M. (1998) *Folding Des. 1*, R95−R106.
4. Neri, D., Billeter, M., Wider, G., & Wüthrich, K. (1992) *Science 257*, 1559−1563.
5. Alexandrescu, A. T., Abeygunawardana, C., & Shortle, D. (1994) *Biochemistry 33*, 1063−1072.
6. Arcus, V. L., Vuilleumier, S., Freund, S. M. V., Bycroft, M., & Fersht, A. R. (1994) *Proc. Natl. Acad. Sci. U.S.A. 91*, 9142−9146.
7. Logan, T. M., Theriault, Y., & Fesik, S. W. (1994) *J. Mol. Biol. 236*, 637−648.
8. Buck, M., Schwalbe, H., & Dobson, C. M. (1995) *Biochemistry 34*, 13219−13232.
9. Frank, M. K., Clore, G. M., & Gronenborn, A. M. (1995) *Protein Sci. 4*, 2605−2615.
10. Pan, H., Barbar, E., Barany, G., & Woodward, C. (1995) *Biochemistry 34*, 13974−13981.
11. Zhang, O., & Forman-Kay, J. D. (1995) *Biochemistry 34*, 6784−6794.
12. Wong, K. B., Freund, S. M. V., & Fersht, A. R. (1996) *J. Mol. Biol. 259*, 805−818.
13. Schwalbe, H., Fiebig, K. M., Buck, M., Jones, J. A., Grimshaw, S. B., Spencer, A., Glaser, S. J., Smith, L. J., & Dobson, C. M. (1997) *Biochemistry 36*, 8977−8991.
14. Zhang, O., Kay, L. E., Shortle, D., & Forman-Kay, J. D. (1997) *J. Mol. Biol. 272*, 9−20.

15. von Bodman, S. B., Schulder, M. A., Jollie, D. R., & Sligar, S. G. (1986) *Proc. Natl. Acad. Sci. U.S.A. 83*, 9443−9447.
16. Ito, A., & Sato, R. (1968) *J. Biol. Chem. 243*, 4922−4923.
17. Spatz, L. & Strittmatter, P. (1971) *Proc. Natl. Acad. Sci. U.S.A. 68*, 1042−1046.
18. Oshino, N., Imai, Y., & Sato, R. (1971) *J. Biochem. (Tokyo) 69*, 155−167.
19. Strittmatter, P., Spatz, L., Corcoran, D., Rogers, M. J., Setlow, B., & Redline, R. (1974) *Proc. Natl. Acad. Sci. U.S.A. 71*, 4565−4569.
20. Hildebrandt, A., & Estabrook, R. W. (1971) *Arch. Biochem. Biophys. 143*, 66−79.
21. Hegesh, E., Hegesh, J., & Kaftory, A. (1986) *New Engl. J. Med. 314*, 757−761.
22. Strittmatter, P., & Ozols, J. (1966) *J. Biol. Chem. 241*, 4787−4792.
23. Banci, L., Bertini, I., Ferroni, F., & Rosato, A. (1997) *Eur. J. Biochem. 249*, 270−279.
24. Arnesano, F., Banci, L., Bertini, I., & Felli, I. C. (1998) *Biochemistry 37*, 173−184.
25. Arnesano, F., Banci, L., Bertini, I., Felli, I. C., & Koulougliotis, D. (1998) (submitted for publication).
26. Dangi, B., Sarma, S., Yan, C., Banville, D. L., & Guiles, R. D. (1998) *Biochemistry 37*, 8289−8302.
27. Pfeil, W., & Bendzko, P. (1980) *Biochim. Biophys. Acta 626*, 73−78.
28. Bendzko, P., & Pfeil, W. (1983) *Biochim. Biophys. Acta 742*, 669−676.
29. Kitagawa, T., Sugiyama, T., & Yamano, T. (1982) *Biochemistry 21*, 1680−1686.
30. Newbold, R. J., Hewson, R., & Whitford, D. (1992) *FEBS Lett. 314*, 419−424.
31. Tajima, S., Enomoto, K., & Sato, R. (1976) *Arch. Biochem. Biophys 172*, 90−97.
32. Bhuyan, A. K., & Udgaonkar, J. B. (1998) *Biochemistry 37*, 9147−9155.
33. Van Nuland, N. A. J., Meijberg, W., Warner, J., Forge, V., Scheek, R. M., Robillard, G. T., & Dobson, C. M. (1998) *Biochemistry 37*, 622−637.
34. Piotto, M., Saudek, V., & Sklenar, V. (1992) *J. Biomol. NMR 2*, 661−666.
35. Marion, D., & Wüthrich, K. (1983) *Biochem. Biophys. Res. Commun. 113*, 967−974.
36. Eccles, C., Güntert, P., Billeter, M., & Wüthrich, K. (1991) *J. Biomol. NMR 1*, 111−130.
37. Güntert, P., Braun, W., & Wüthrich, K. (1991) *J. Mol. Biol. 217*, 517−530.
38. Bertini, I., & Luchinat, C. (1986) in *NMR of paramagnetic molecules in biological systems*, Benjamin/Cummings, Menlo Park, CA.
39. Bertini, I., & Turano, P. (1994) in *NMR of paramagnetic macromolecules* (La Mar, G. N., Ed.) NATO ASI Series, Kluwer Academic Publishers, Dordrecht, The Netherlands.
40. Bertini, I., & Luchinat, C. (1996) in *NMR of paramagnetic substances*, Coordination Chemistry Review 150, Elsevier, Amsterdam.
41. Gochin, M., & Roder, H. (1995) *Protein Sci. 4*, 296−305.
42. Banci, L., Bertini, I., Cremonini, M. A., Gori Savellini, G., Güntert, P., Luchinat, C., & Wüthrich, K. (1998) *J. Biomol. NMR* (in press).
43. Güntert, P., Mumenthaler, C., & Wüthrich, K. (1997) *J. Mol. Biol. 273*, 283−298.
44. Banci, L., Bertini, I., Bren, K. L., Cremonini, M. A., Gray, H. B., Luchinat, C., & Turano, P. (1996) *JBIC 1*, 117−126.
45. Banci, L., Bertini, I., Gori Savellini, G., Romagnoli, A., Turano, P., Cremonini, M. A., Luchinat, C., & Gray, H. B. (1997) *Proteins*: *Struct., Funct., Genet. 29*, 68−76.
46. Pearlman, D. A., Case, D. A., Caldwell, J. W., Ross, W. S., Cheatham, T. E., Ferguson, D. M., Seibel, G. L., Singh, U. C., Weiner, P. K., & Kollman, P. A. (1995) *AMBER 4.1*, University of California, San Francisco, CA.
47. Banci, L., Bertini, I., Gray, H. B., Luchinat, C., Reddig, T., Rosato, A., & Turano, P. (1997) *Biochemistry 36*, 9867−9877.
48. Laskowski, R. A., MacArthur, M. W., Moss, D. S., & Thornton, J. M. (1993) *J. Appl. Crystallogr. 26*, 283−291.
49. Laskowski, R. A., Rullmann, J. A. C., MacArthur, M. W., Kaptein, R., & Thornton, J. M. (1996) *J. Biomol. NMR 8*, 477−486.
50. Borgias, B., Thomas, P. D., & James, T. L. (1989) *COmplete Relaxation Matrix Analysis (CORMA)*, University of California, San Francisco, CA.
51. Santoro, M. M., & Bolen, D. W. (1988) *Biochemistry 27*, 8063−8068.
52. Agashe, V. R., & Udgaonkar, J. B. (1995) *Biochemistry 34*, 3286−3299.
53. Wüthrich, K. (1986) in *NMR of Proteins and Nucleic Acids*, Wiley, New York.
54. Kabseh, W., & Sander, C. (1983) *Biopolymers 22*, 2577−2637.
55. Reid, L. S., Mauk, M. R., & Mauk, A. G. (1984) *J. Am. Chem. Soc. 106*, 2182−2185.
56. Funk, W. D., Lo, T. P., Mauk, M. R., Brayer, G. D., MacGillivray, R. T. A., & Mauk, A. G. (1990) *Biochemistry 29*, 5500−5508.
57. Mathews, F. S., Argos, P., & Levine, M. (1972) *Cold Spring Harbor Symp. Quant. Biol. 36*, 387.
58. Banci, L., Bertini, I., Cavazza, C., Felli, I. C., & Koulougliotis, D. (1998) *Biochemistry 37*, 12320−12330.
59. Bai, Y. W., Sosnick, T. R., Mayne, L., & Englander, S. W. (1995) *Science 269*, 192−197.
60. Roder, H., & Elöve, G. A. (1994) in *Mechanisms of Protein Folding: Frontiers in Molecular Biology* (Pain, R. H., Ed.) pp 26−55, Oxford University Press, New York.
61. Nall, B. T., & Landers, T. A. (1981) *Biochemistry 20*, 5403−5411.
62. Zuniga, E. H., & Nall, B. T. (1983) *Biochemistry 22*, 1430−1437.
63. Sauder, J. M., MacKenzie, N. E., & Roder, H. (1996) *Biochemistry 35*, 16852−16862.
64. Colón, W., Elöve, G. A., Wakem, L. P., Sherman, F., & Roder, H. (1996) *Biochemistry 35*, 5538−5549.
65. Elöve, G. A., Bhuyan, A. K., & Roder, H. (1994) *Biochemistry 33*, 6925−6935.
66. Banci, L., Berners-Price, S., Bertini, I., Clementi, V, Luchinat, C., Spyroulias, G. A., & Turano, P. (1998) *Mol. Phys.* (in press).
67. Bushnell, G. W., Louie, G. V., & Brayer, G. D. (1990) *J. Mol. Biol. 214*, 585−595.
68. Koradi, R., Billeter, M., & Wüthrich, K. (1996) *J. Mol. Graphics 14*, 51−55.

BI981546P